ORIGINAL

Improving gas permeability and characterizing the multi-scale pore size distribution of radiata pine (*Pinus radiata* D. Don) treated via high-intensity microwave

Xuefeng Xing[1,2,3] · Shanming Li[1,3] · Juwan Jin[2] · Lanying Lin[1] · Yongdong Zhou[1] · Limin Peng[1] · Feng Fu[1]

Abstract

The effects of different microwave energy densities (0, 60, 80, and 100 kWh/m^3) on the gas permeability of sapwood and heartwood of radiata pine in the longitudinal, radial, and tangential directions were investigated. The multi-scale pore size distribution was systematically analyzed with various analytical methods. High intensity microwave (HIMW) treatment significantly improved the gas permeability of the wood in three directions, and the gas permeability was positively correlated with the microwave energy density. The gas permeability of the treated sapwood was 1.6–2.5 times higher, and that of the treated heartwood was more than 6 times higher than the untreated wood at the microwave energy density of 100 kWh/m^3. The HIMW treatment significantly affected the pore size distribution. In the micropore–mesopore (< 50 nm) range, the surface area and average pore diameter of the treated sapwood samples were 10.68% and 17.12% higher, respectively, and the total pore volume was 31.50% lower than that of the untreated sample. However, the specific surface area and total pore volume of the heartwood samples were 14.92% and 26.06% lower, respectively, and the average pore diameter was 35.55% higher at the microwave energy density of 100 kWh/m^3. Treated wood mainly had slit-shaped mesopores (< 10 nm). For macropores (> 50 nm), treated sapwood displayed 20.57% total pore volume increase and 11.66% porosity rise; treated heartwood showed 31.24% total pore volume rise and 20.78% porosity increment. Furthermore, SEM results showed HIMW treatment damaged weak structures like the compound middle lamella and ray parenchyma cells.

✉ Shanming Li
  lishanming@caf.ac.cn

[1] Research Institute of Wood Industry, Chinese Academy of Forestry, Beijing, China

[2] College of Materials Science and Engineering, Nanjing Forestry University, Nanjing, China

[3] Co-Innovation Center of Efficient Processing and Utilization of Forest Resources, Nanjing Forestry University, Nanjing, China
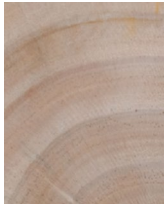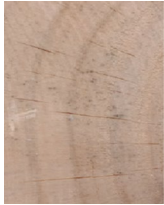
Introduction

Radiata pine is the dominant species of softwood logs and timber imported to China. It is widely used for manufacturing furniture and wood-based composites. However, some properties, such as low density and low decay resistance, limit its application as structural components and outdoor materials. Therefore, wood modification treatments, such as heat treatment, impregnation modification, and other technologies, have been employed to enhance wood properties aiming to enable the multifunctional applications of radiata pine wood (Boonstra et al. 2007). Nevertheless, the low permeability of radiata pine wood (especially heartwood) increases both drying cycles and defects of sawn timber and reduces the penetration degree of functional agents. Therefore, it is necessary to improve the permeability of radiata pine to expand its application. Research on this subject has focused on microbial erosion, chemical degradation, ultrasonic, supercritical carbon dioxide, and microwave treatments (Jang and Kang 2019; Lehringer et al. 2009; Tanaka et al. 2010; Torgovnikov and Vinden 2009).

Microwave treatment of wood is efficient for the mass production of large samples. The heat from the microwaves polarizes and rotates the water molecules in wood, generating a large amount of heat due to friction (Yongsawatdigul and Gunasekaran 1996). The chemical composition in wood cell walls changes under the heat, which affects wood mechanical properties (Wang et al. 2022). When the vapor pressure inside the wood surpasses the strength of weak tissues (such as microfibrils, pit membranes, compound middle lamellae, and ray parenchyma cells), it will cause micro-mesoscopic damage to wood cells or tissues. This can potentially result in the formation of macroscopic cracks, consequently enhancing the wood permeability (Torgovnikov and Vinden 2009; Weng et al. 2020). Torgovnikov et al. conducted a systematic study on the influence of microwave treatments on the wood structure. The damage level caused by the microwave treatment was divided into seven categories (Torgovnikov and Vinden 2010). The treated wood samples were then impregnated with a copper naphthenate solution, creosote, and copper chromium arsenic to prepare preservative railway sleepers (Vinden et al. 2011). Other researchers classified microwave-treated wood into three types based on the wood volume expansion rate, the level of wood damage, and the decrease in mechanical strength (Xu et al. 2020). The classification is listed in Table 1. Although a normative evaluation of the effect of the high-intensity microwave (HIMW) treatment has been conducted, most studies focused on changes in the microstructure or single-scale pore size. Therefore, comprehensive investigations into the multi-scale pore size distribution of HIMW-treated wood are notably absent from the existing research.

Wood is a porous material consisting of macro-capillary and micro-capillary systems (Hao et al. 2020). The pore size distribution of wood determines its processing quality, such as the drying rate, mechanical strength, and permeability of modifiers. It also significantly affects the environmental properties of wood products, such as thermal insulation and sound absorption performance (Fan et al. 2022; Jang and Kang 2019). According to the International Union of Pure

Table 1 Quality classification of HIMW-treated wood

	Type I	Type II	Type III
Macro-features			
Volume expansion ratio (%)	≤4	4–9	≥9
Fracture area ratio (%)	≤7	7–14	≥14
Number of cracks (PCS/m^2)	≤3000	3000–6000	≥6000
Bending strength reduction rate (%)	≤5	5–15	≥15
Structural changes	Disruption of the pit membrane, reduction in the number of occluded pits; redistribution of the extractives[a]	Destruction of ray cells, axial parenchyma cells, and cell wall compound middle lamella[b]	Thick-walled cells such as tracheids and wood fibers were damaged and obvious macroscopic cracks appeared[c, d]
Functional utilization	Increasing permeability and drying speed [e, f]	Impregnation treatment of high molecular weight modifiers, such as preservatives and flame retardants[g, h]	Impregnation, high thermal conductivity, and other functional composite treatments with viscous modifiers[i]

[a](Kol and Çayır. 2023); [b](Ganguly et al. 2021); [c](Weng et al. 2020); [d](He et al. 2014); [e](Song et al. 2016); [f](Farajollah et al. 2021); [g](Poonia et al. 2016); [h](Ramezanpour et al. 2015); [i](Chai et al. 2020)

and Applied Chemistry (IUPAC), the pore size of wood is commonly divided into three types: micropores (pore diameter < 2 nm), mesopores (pore diameter 2–50 nm) and macropores (pore diameter > 50 nm) (Jang et al. 2020; Jang and Kang 2019; Yin et al. 2015). Yin et al. (2015) categorized the pore types in wood according to the pore size. Micropores are gaps among microcrystals, microfibrils, and fibrils in the cell walls, and their average diameter is 1.0–4.5 nm (Li et al. 2021). Mesopores mainly consist of slit-shaped pores on the dry or wet cell walls, including smaller pores in bordered pit membranes (Kaack et al. 2019). Micropores and mesopores in wood cell walls have been proved to affect adsorption performance, mechanical properties, and weather resistance of wood (Kojiro et al. 2010; Östlund et al. 2010). Macropores encompass cell cavities and pits on the cell walls, including vessels and fiber cavities within hardwood, as well as tracheid cavities, resin canals, and bordered pits within softwood. Macropores are the main channel for the movement of liquid and gaseous substances in wood. However, their adsorption performance and capacity to retain absorbed substances are found to be less potent compared with mesopores (Abe et al. 2001).

Numerous sophisticated analytical techniques have been developed for directly or indirectly characterizing the pore size distribution of wood. Among the direct methods are microscopic imaging techniques such as computed tomography (CT), scanning electron microscopy (SEM), transmission electron microscopy (TEM), atomic force microscopy (AFM), and optical microscopy. These methods allow for the observation and quantification of pores (Grigsby et al. 2013; Zauer et al. 2014). Indirect approaches, on the other hand, encompass techniques like Brunauer–Emmett–Teller (BET) analysis of gas adsorption data (N_2 BET, CO_2 BET), mercury intrusion porosimetry (MIP), differential scanning calorimetry (DSC), and low-temperature nuclear magnetic resonance (NMR). These methods have been widely used to determine the multi-scale pore size distribution of wood materials (Grigsby et al. 2013; Zauer et al. 2014). As
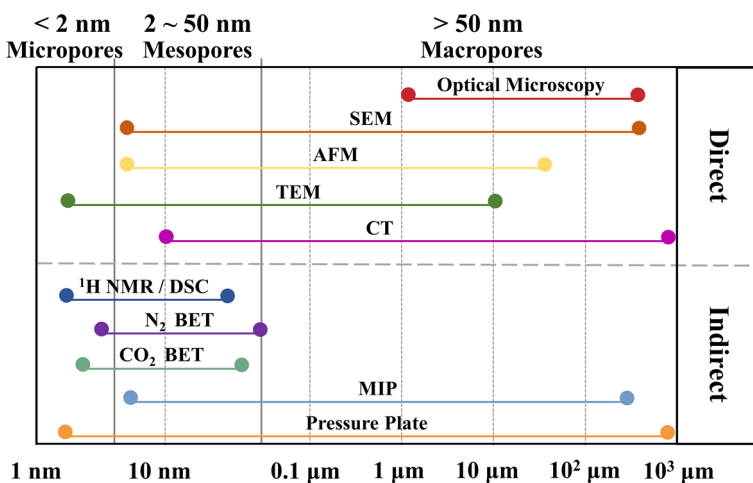

Fig. 1 Testing methods for analyzing pore size distribution and typical ranges

shown in Fig. 1 (Anovitz and Cole 2015; Giacomozzi et al. 2019), divers testing methods possess distinct application conditions and characterization ranges because of different test principles. Therefore, a single test method has limitations for characterizing multi-scale pore size distributions. However, due to the intricate nature of wood's pore size distribution and pore network, a more comprehensive understanding of the pore system in wood materials can be achieved by employing multiple testing methods that leverage their complementary characteristics.

In general, one main purpose of the study is to investigate the effect of HIMW treatment on the gas permeability of radiata pine sapwood and heartwood at different microwave energy densities. In addition, a comprehensive approach involving nitrogen adsorption–desorption (NAD) analysis, ^{1}H NMR, MIP and SEM was adopted to analyze the impact of HIMW treatment on the pore size distribution of both sapwood and heartwood, spanning from the microscale to the macroscale. Through these analyses, the mechanism of the HIMW treatment on the wood structure was elucidated. It is hoped that this research will provide valuable guidance for the efficient drying and subsequent functional improvement of radiata pine wood. Simultaneously, the study aims to provide theoretical insights that can drive the further development of HIMW treatment, ultimately facilitating the high-value utilization of wood materials.

Materials and methods

Materials and HIMW treatment

A New Zealand radiata pine (*Pinus radiata* D. Don) log, with a length of 2 m, a diameter of 450 mm at breast height, and an age of 23 years, was used in this study. The log was sawn into lumber pieces with dimensions of 800 mm $(L) \times 90$ mm $(T) \times 50$ mm (R). The pieces were categorized into sapwood (S) and heartwood (H). The densities of the sapwood and heartwood at 12% moisture content were tested as 0.41 g/cm^3 and 0.47 g/cm^3, respectively. After adjusting the moisture content of the sawn lumber to $60 \pm 10\%$ by the gravimetric method, the pieces were sealed at the ends with epoxy resin adhesive and wrapped in film before being stored in cold storage at -6 °C for further processing.

The HIMW treatment was carried out using a tunnel microwave treatment device (WX20L, Nanjing Sanle Microwave Technology Development Co., Ltd., China). The details of the device have been described by Wang et al. (2022). The effect of the microwave treatment on wood is influenced by several factors, including processing time, microwave power level, and feeding speed. In this study, three energy densities (60, 80, and 100 kWh/m^3) were adopted to treat the radiata pine sapwood and heartwood. Table 2 lists the HIMW treatment parameters for the three groups.

Table 2 HIMW treatment parameters

Power (kW)	Feeding speed (m/min)	Processing time (min)	Microwave energy density (kWh/m³)
16	1.0	2	60
18	0.8	2.5	80
20	0.75	2.7	100

Gas permeability test

As shown in Fig. 2a, the untreated and HIMW-treated lumber was sawn into three types of wood boards with a thickness of 25 mm. Cylindrical samples with a diameter of 25 mm were drilled from these boards. The heights of the three samples were parallel to the longitudinal, radial, and tangential directions of the wood, corresponding to the gas permeability in the longitudinal, radial, and tangential directions, respectively. The samples were placed in a chamber set at a temperature of 20 °C and a relative humidity of 65%, ensuring the moisture content was adjusted to $12 \pm 1\%$. A gas permeability tester (CRIWI-GP-01, Unipac Technology Co., Ltd., China) was employed to measure the gas permeability of the untreated and treated samples in the three directions. During the test, the sample was securely placed within a circular holder surrounded by a rubber ring. A ring pressure of 0.1 MPa was applied around the rubber ring to prevent gas from escaping from the side of the sample. Subsequently, nitrogen gas was introduced into the sample at a certain pressure from the inlet, with the outlet connected to a soap film flowmeter. The volumetric flow rate of the gas was calculated by measuring the start and end times of the soap film's passage through a predefined volume in the glass tube. The gas permeability D_g of the wood was calculated according to Eq. (1), and the test results of each group were the average value of six samples.
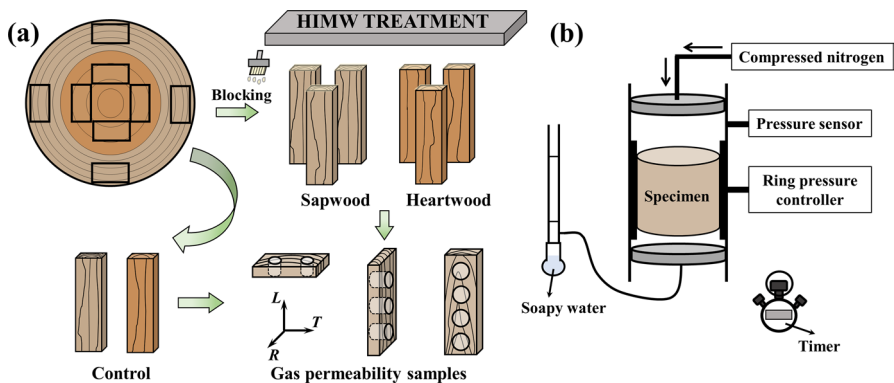
Fig. 2 Schematic diagram of sample preparation for HIMW treatment (**a**) and gas permeability test (**b**)

$$D_g = \frac{2LP_0Q\eta}{A\Delta P(2P_0 + \Delta P)} \tag{1}$$

where D_g is gas permeability (Darcy, m³/m), L the length of the sample parallel to the direction of gas flow (m), P_0 is atmospheric pressure ($P_0 = 1 \times 10^5$ Pa), Q is the gas volume flow (m³/s), η is the viscosity of nitrogen ($\eta = 1.78 \times 10^{-5}$ Pa·s) (Tanikawa and Shimamoto 2009), A is the cross-sectional area (m²), and ΔP is the gas pressure difference applied at both ends of the sample (Pa).

^{1}H NMR relaxometry and cryoporometry

Cylindrical samples, measuring 8 mm in diameter and 20 mm in length along the grain, were obtained near the same annual rings in the center of the untreated and treated wood for ^{1}H NMR testing. The sapwood samples contained two latewood segments and one intact earlywood segment, whereas the heartwood samples contained one intact latewood segment and two earlywood segments. Prior to testing, the samples were immersed in deionized water and treated at 20 °C and a vacuum pressure of 1 MPa for 24 h to ensure that the samples were saturated. The water on the sample surface was wiped off, and the sample was placed in a Teflon NMR sample tube with an outer diameter of 10 mm immediately after weighing. The ^{1}H NMR test was conducted using a low-temperature NMR instrument (NMRC12-010V, Niumag, Instruments, Suzhou, China) boasting a magnetic field strength of 0.5 T and a main frequency of 12 MHz. The test employed the single-scan Carr–Purcell–Meiboom–Gill (CPMG) pulse sequence, with the following acquisition parameters: echo time 0.05 μs, echo number 15,000, and cumulative number 64. In the relaxation test and low-temperature freeze–thaw test, the T_2 relaxation test was initially conducted on the specimen at 20 °C, succeeded by the freeze–thaw test encompassing 11 temperature levels. The cryoporometry test commenced from the lowest temperature. The temperature in the sample chamber was gradually raised to each specific required temperature after reaching the minimum of −40 °C. Upon the sensor temperature aligning with the preset value, it remained constant for 2 h, during which the T_2 scan was performed. Following the completion of all measurements, the analysis software provided with the instrument was utilized to carry out T_2 inversion. For the determination of the theoretical pore size distribution of wood cell walls, the Gibbs–Thomson thermodynamic equation was used. This was based on the low-temperature NMR freeze–thaw method (Furó and Daicic 1999). It was assumed that the wood cells and the pores on the cell walls took a cylindrical shape. With rising temperature, the content of adsorbed water within wood cell walls progressively increased. Consequently, there was an increase in the intensity of ^{1}H relaxation signal, indicating the gradual accumulation process of pore volume within the wood cell wall structure, progressing from small to large. This correlation is illustrated in Eq. (2), where the melting point of the liquid in the wood cells demonstrates a positive relationship with the pore size.

$$\Delta T_{\mathrm{m}} = T_{\mathrm{m}} - T_{\mathrm{m}}(D) = \frac{4\gamma T_{\mathrm{m}} \cos\theta}{D\rho\Delta H_{\mathrm{f}}} \tag{2}$$

where T_{m} is the melting temperature ($T_{\mathrm{m}} = 273.15$ K), $T_{\mathrm{m}}(D)$ is the freezing temperature of a pore with the diameter D (K), D is the pore diameter (nm), γ is the water–ice interface free energy ($\gamma = 12.1$ mJ/m^2) (Park et al. 2006), ρ is the density of water ($\rho = 1.0 \times 10^3$ kg/m^3), H_{f} is the specific heat of fusion of freezing bound water ($H_{\mathrm{f}} = 334$ J/g) (Maloney et al. 1998), and θ is the contact angle ($\theta = 180°$). Furthermore, considering that the nonfreezing monolayer of water molecules gets adsorbed at the ice–solid interface, an adjustment is required for the theoretical diameter (Cao et al. 2021; Gao et al. 2015; Kekkonen et al. 2014; Telkki et al. 2013). The corrected relationship between melting temperature and pore size is presented in Table 3.

Nitrogen adsorption–desorption (NAD) tests

The untreated and treated wood samples were ground into a fine powder with diameters of 0.25–0.42 mm (40–60 mesh) and dried in an oven at 60 °C until completely dry. A high-speed automated surface area and pore size analyzer (ASAP 2460, Micromeritics, Inc., Norcross, GA, USA) was employed in the test. The powder sample was degassed for 12 h at constant pressure in an environment with a temperature of 40 °C and a vacuum of less than 7×10^{-2} Pa to remove gas and water molecules from the sample surface. The NAD test was performed on samples weighing 2–3 g at a temperature of 77.4 K using nitrogen as the adsorption medium. The relative pressure (p/p_0) range of the test was 0.01–0.99 (where p is the system's internal gas vapor pressure, and p_0 is the saturated vapor pressure of liquid nitrogen at 77 K). The BET molecular model was used to calculate the surface areas of the micropores and mesopores (<50 nm), and the Barrett–Joyner–Halenda (BJH) model was used to evaluate the pore size distribution of the mesopores (Liang et al. 2020). Each group's result was determined by averaging the outcomes of two separate tests.

Table 3 Melting temperature versus pore diameters in the cryoporometry test

Melting temperature $T_{\mathrm{m}}(D)$ (℃)	Theoretically calculated pore diameter (nm)	Corrected pore diameter (nm)
− 40	0.99	1.59
− 30	1.32	1.92
− 25	1.58	2.18
− 20	1.98	2.58
− 15	2.64	3.24
− 10	3.96	4.56
− 8	4.95	5.55
− 5	7.92	8.52
− 4	9.9	10.50
− 3	13.2	13.80
− 1	39.6	40.20

Mercury intrusion porosimetry (MIP) test

The MIP samples were obtained from the same growth rings as the other untreated and treated wood samples to ensure the equivalent wood structure. The size of the MIP sample was 5 mm $(L) \times 15$ mm $(T) \times 15$ mm (R). The sapwood samples contained three latewood segments and two earlywood segments (7th to 9th growth ring) and the heartwood samples contained one latewood segment and two earlywood segments (18th to 19th growth ring). The samples were dried at 60 °C until they achieve complete dryness. A high-performance automated mercury porosimeter (AutoPore V9620, McMeritick Company, USA) was employed to test the pore size distribution and porosity of the macroscopic pores (> 50 nm). The samples were immersed in mercury, and the pressure was increased from 0.5 psia to 35,000 psia. With the gradual increase in pressure, mercury gradually penetrated the smaller pores. The relationship between the pressure and the pore size distribution of the wood was determined using the Washburn equation (Eq. 3) (Muller and Scrivener 2017). Two samples from the same group were tested simultaneously, and their average value was taken as result for the group.

$$d = -\frac{4\gamma_{\text{Hg}}\cos\theta}{p} \tag{3}$$

where d is the pore diameter (nm), θ is the contact angle of mercury ($\theta = 141°$), γ_{Hg} is the surface tension of mercury ($\gamma_{\text{Hg}} = 0.48$ N/m) (Junghans et al. 2005), and p is the measured pressure.

Scanning electron microscopy (SEM)

The untreated and treated sapwood and heartwood samples were trimmed with a microtome (HistoCore MULTICUT, Leica, Wetzlar, Germany) to obtain the optimal sample surface. The dried samples were mounted on a specific disk with a conductive carbon adhesive tab and coated with gold for 60 s using a vacuum sputtercoater (EM ACE600, Leica, Germany) to improve the quality of the SEM images. The transverse, radial, and tangential sections of the samples were analyzed by SEM (Regulus SU8230, Hitachi, Japan).

Results and discussion

Results of gas permeability test

The longitudinal, radial, and tangential gas permeabilities of radiata pine sapwood and heartwood before and after HIMW treatment are shown in Fig. 3. The gas permeabilities of untreated sapwood in the longitudinal, radial, and tangential directions were determined as 8.90×10^{-14} m^3/m, 5.93×10^{-14} m^3/m, and 4.28×10^{-14} m^3/m, whereas those of the untreated heartwood were 3.21×10^{-14} m^3/m, 1.85×10^{-14} m^3/m,
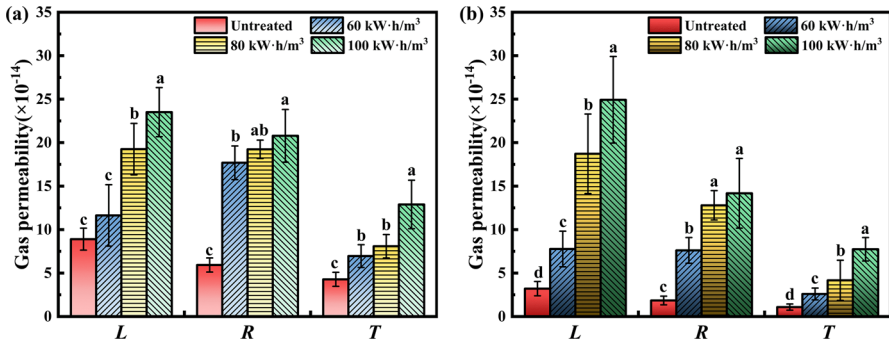
Fig. 3 Gas permeabilities of untreated and HIMW-treated samples. Sapwood (**a**); Heartwood (**b**). * L, R, T represent the test samples in longitudinal, radial, and tangential directions, respectively. *Different letters represent significant differences between samples ($p < 0.05$)

and 1.08×10^{-14} m³/m, respectively. The gas permeability of sapwood was higher than that of heartwood, which was consistent with previous research on the gas permeability of softwood (Jang et al. 2020). Due to the anatomical structure, the longitudinal gas permeability of radiata pine wood is the highest, and the gas permeability is slightly higher in the radial direction than in the tangential direction. Clearly, the HIMW treatment significantly increased the gas permeability of wood in the three directions ($p < 0.05$). The gas permeability of the radiata pine sapwood and heartwood increased with an increase in microwave energy density. At a microwave energy density of 100 kWh/m³, the gas permeabilities of the sapwood in the three directions were 2.35×10^{-13} m³/m, 2.08×10^{-13} m³/m, and 1.29×10^{-13} m³/m, respectively. These values were 164.04%, 250.76%, and 201.40% higher than those of the untreated wood. Under these three conditions, the HIMW treatment did not result in any visible damages to radiata pine sapwood. Thus, the increase in the gas permeability of the sapwood can be attributed to the induced damages to the cell wall microstructure. The improvement in gas permeability following HIMW treatment was more significantly pronounced in the case of heartwood compared to sapwood. The gas permeabilities of the heartwood in the three directions at the energy density of 100 kWh/m³ were measured as 2.49×10^{-13} m³/m, 1.42×10^{-13} m³/m and 0.77×10^{-13} m³/m, respectively. These figures represented remarkable improvements of 675.70%, 667.57%, and 612.96%, respectively, compared to the untreated samples. Specifically, visible cracks were observed on the surfaces of heartwood samples treated at both energy densities of 80 kWh/m³ and 100 kWh/m³. Under these two energy levels, the HIMW treatment led to notable structural damages in wood, which consequently increased the internal channels in the samples and significantly enhanced the gas permeabilities.

Changes in wood morphology

The morphological changes of radiata pine sapwood and heartwood before and after HIMW treatment are shown in Figs. 4 and 5, respectively. Among the wood
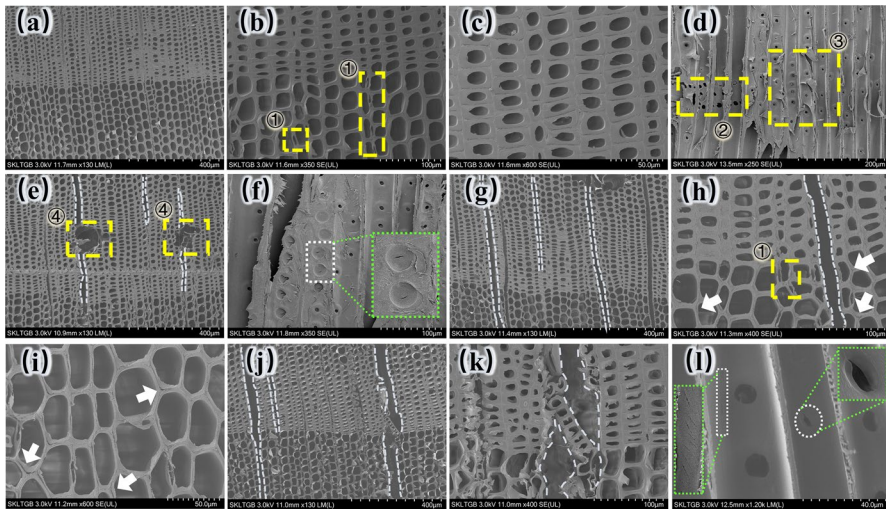
Fig. 4 SEM images of untreated and HIMW-treated sapwood samples. Transverse sections of untreated sapwood sample at 130×, 400×, and 600×magnifications, respectively (**a–c**); radial section of untreated sapwood sample at 600×magnification (**d**); transverse and radial sections of 60 kWh/m^3 treated sample at 130×and 350×magnifications, respectively (**e–f**); transverse sections of 80 kWh/m^3 treated sample at 130×, 400×, and 600×magnifications, respectively (**g–i**); transverse sections of 100 kWh/m^3 treated sample at 130×and 400×magnifications (**j–k**); radial section of 100 kWh/m^3 treated sample at 1200×magnification (**l**). The dotted line shows the fracture along the radial direction caused by HIMW treatment; the image in the dashed box shows the partial enlarged view; the arrow indicates the split of cell wall layers caused by HIMW treatment. Pit chambers ①; cross-field pits ②; bordered pits ③; axial resin canals ④

microstructures possessing weak mechanical strength, ray parenchyma cells were the first ones to be destroyed during the HIMW treatment, resulting in the formation of cracks that extended in the radial direction in the transverse section. When the microwave energy density exceeded 80 kWh/m^3, a pronounced rupture of wood rays became evident, as illustrated in Fig. 5g–h, and this phenomenon was particularly obvious in the treated heartwood samples. Under the effect of the internal vapor pressure in the treated wood, the cell wall layers adjacent to wood rays were pulled apart. As shown in Figs. 4 and 5, the cell wall layers of the compound middle lamella (CML) between the tracheids were destroyed, and splits were observed in the outer layer of the secondary wall (S1) and the middle layer of the secondary wall (S2), denoted by the arrows. In addition, the bordered pit membranes and pit borders in the radial tracheid walls were broken in the treated sapwood and heartwood samples (Fig. 4 f), and the cross-field pits of the ray parenchyma cells and tracheids were cracked (Figs. 4l and 5j–k). Notably, a similar failure mode was also reported by Weng et al. (2020), who performed an HIMW treatment of Chinese fir. When the microwave energy density was further increased to 100 kWh/m^3, the tracheid walls underwent further splitting, and these cracks extended in the microfibril direction of the S2 layer (Figs. 4l and 5l). The fractures of the wood ray parenchyma cells, pits (bordered pits and cross-field pits), and tracheid walls, as induced by HIMW treatment, significantly improved the transmission and permeability of gas or liquid in
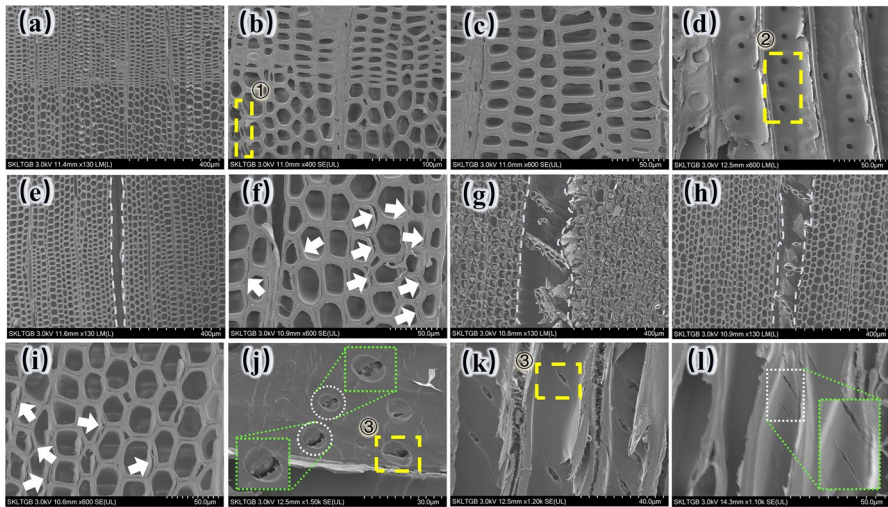
Fig. 5 SEM images of untreated and HIMW-treated heartwood samples. Transverse sections of untreated heartwood sample at $130\times$, $400\times$, and $600\times$ magnifications, respectively (**a–c**); radial section of untreated sample at $600\times$ magnification (d); transverse sections of 60 kWh/m^3 treated sample at $130\times$ and $600\times$ magnifications, respectively (**e–f**); transverse section of 80 kWh/m^3 treated sample at $130\times$ magnification (**g**); transverse sections of 100 kWh/m^3 treated sample at $130\times$ and $600\times$ magnifications (**h–i**); radial sections of 100 kWh/m^3 treated sample at $1500\times$ and $1200\times$ magnifications (**j–k**); tangential section of 100 kWh/m^3 treated sample at $1100\times$ magnification (**l**). The dotted line shows the fracture along the radial direction caused by HIMW treatment; the image in the dashed box shows the partial enlarged view; the arrow indicates the split of cell wall layers caused by HIMW treatment. Pit chambers ①; bordered pits ②; cross-field pits ③

the transverse (radial and tangential) direction of the wood. This aspect is detailed in Sect. "Results of gas permeability test".

Distributions of micropores and mesopores

In order to explore the effect of HIMW treatment on the micro-mesoporous distribution in wood cell walls, NAD and ^{1}H NMR analyses were used in this section. The results of the NAD isotherms of HIMW treated and untreated radiata pine sapwood and heartwood samples are displayed in Fig. 6. The configuration of the adsorption–desorption isotherm indicates the pore shape and wood structure concerning the micro-mesopores (Yang et al. 2023). A very narrow hysteresis loop was observed between the adsorption and desorption isotherms. According to the IUPAC classification, the hysteresis loops of all the samples conform to the H3 type (Yin et al. 2015), which is related to the capillary condensation and evaporation in the mesopores. The results showed that both untreated and treated samples predominantly contained slit-shaped pores (Sang et al. 2018). At low relative pressure ($p/p_0 < 0.1$), the adsorption isotherm exhibited a gradual ascent, indicating the presence of micropores in all the samples. As the relative pressure increased further ($p/p_0 > 0.9$), the adsorption capacity increased rapidly
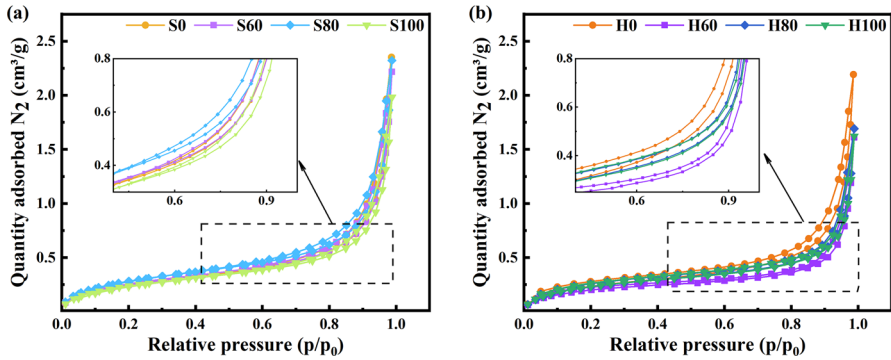
Fig. 6 N_2 adsorption–desorption isotherms of untreated and HIMW treated samples. Sapwood (**a**); Heartwood (**b**)

and did not reach saturation, indicating that capillary condensation occurred in larger mesopores and macropores (Wang et al. 2014). Therefore, it could be concluded that micropores, mesopores, and macropores were prevalent in both untreated and treated samples. The results also demonstrated that the morphology of the micropores and mesopores remained relatively unaffected by the HIMW treatment.

Table 5 lists the specific surface area, specific pore volume, and average pore diameter. Notably, the BET surface area, total pore volume, and BJH average pore diameter exhibited higher values in the untreated sapwood in comparison with the untreated heartwood. The surface areas of the sapwood and heartwood were 0.9720 m^2/g and 0.8996 m^2/g. The total pore volumes were 3.638×10^{-3} cm^3/g for sapwood and 3.393×10^{-3} cm^3/g for heartwood, while the BJH average pore diameters were 15.0238 nm for sapwood and 14.4327 nm for heartwood, respectively. The difference in the pore characteristics between sapwood and heartwood in the micro-mesopore range was consistent with the results of Yin et al. (2015),

Table 5 Micro-mesopore characteristics of untreated and treated samples measured by NAD

Sample	BET Surface area (m^2/g)	Total intrusion volume (cm^3/g)	BJH Average pore diameter (nm)
S0	0.9720 ± 0.0141	0.003638 ± 0.000058	15.0238 ± 0.083
S60	0.9997 ± 0.0674	0.003430 ± 0.000078	15.4353 ± 0.093
S80	0.9308 ± 0.0156	0.003593 ± 0.000106	15.9961 ± 0.086
S100	1.0758 ± 0.0707	0.003066 ± 0.000021	17.5954 ± 0.111
H0	0.8996 ± 0.0949	0.003392 ± 0.000057	14.4327 ± 0.176
H60	0.8861 ± 0.0853	0.002492 ± 0.000053	15.5827 ± 0.091
H80	0.9096 ± 0.0071	0.002617 ± 0.000121	17.2586 ± 0.131
H100	0.7654 ± 0.0166	0.002508 ± 0.000129	19.5632 ± 0.134

*Data were expressed as averages $\pm$ SD

and this distinction was related to the different physiological functions of heartwood and sapwood (Bamber 1976).

After the HIMW treatment, variations were observed in the pore characteristics between sapwood and heartwood samples. The BET surface area and BJH average pore diameter of treated sapwood increased slightly, while the total pore volume decreased slightly in response to the increase in the microwave energy density. Specifically, the BET surface area and BJH average pore diameter of the sapwood samples treated at an energy density of 100 kWh/m^3 were 10.68% and 17.12% higher, while the total pore volume was 15.72% lower than that of the untreated sapwood. The alteration can likely be attributed to the deformation and destruction of sapwood cell walls induced by HIMW treatment, consequently leading to the formation of new micropores (Bao et al. 2017). These micropores are depicted in Fig. 4.

As the microwave energy density increased, the pore characteristics of the heartwood did not exhibit a monotonic trend. However, the BET surface area and total pore volume of treated heartwood samples decreased, whereas the BJH average pore diameter increased significantly. Heartwood samples treated at 100 kWh/m^3 had a BET surface area of 0.7654 m^2/g and a total pore volume of 2.508×10^{-3} cm^3/g, respectively, which were 14.92% and 26.06% lower than the untreated heartwood. The BJH average pore diameter was 19.5632 nm, marking an increase of 35.55% compared with the untreated heartwood. The main reason was that the HIMW treatment destroyed the micropores and mesopores in the cell walls of the heartwood (He et al. 2014; Terziev et al. 2020; Weng et al. 2020), resulting in a significant increase in pore size.

These results showed that the effect of the HIMW treatment on the pore size characteristics of the micropores and mesopores was more significant in the heartwood samples than in the sapwood samples. This difference can be attributed to the fact that the HIMW treatment induced a higher vapor pressure within heartwood due to its lower permeability, which led to more substantial cell wall damages in heartwood. Consequently, the gas permeability of heartwood samples displayed a significant enhancement following the HIMW treatment.

Figure 7 displays the relationship between the log-differential pore volume and pore size distribution of radiata pine sapwood and heartwood before and after the HIMW treatment obtained from NAD. The micro-mesopore distribution of the sapwood and heartwood was significantly different, consistent with the research results of Yin et al. (2015). The curves of the sapwood in the mesopore region are relatively smooth, whereas those of the heartwood are highly variable, with multiple peaks in the range of 6–10 nm. In addition, the sapwood exhibited fewer micropores but more mesopores in comparison with the heartwood, resulting in a higher BET surface area, total pore volume, and BJH average pore diameter of the sapwood (Table 5). As shown in Fig. 7a, the peaks in the 2–5 nm range of the sapwood sample shifted slightly to the left after the HIMW treatment, indicating that the pore size of the treated sample was slightly larger for a diameter of less than 5 nm. At an energy density of 100 kWh/m^3, the pore diameter of the sapwood was substantially larger than that of the untreated sample for a diameter below 15 nm. As shown in Fig. 7b, the HIMW treatment had a significant effect on the micro-mesopore pore size distribution of the heartwood sample, especially in the range of 2–10 nm. The sample treated
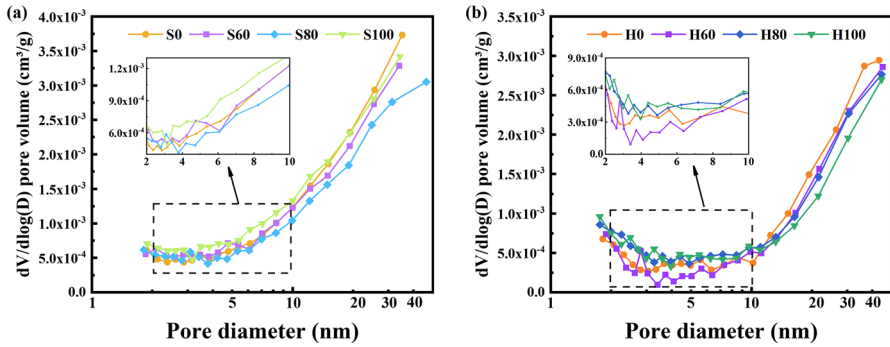
Fig. 7 Micro-mesopore size distributions of untreated and HIMW-treated samples measured by NAD. Sapwood (**a**); Heartwood (**b**)

at the energy density of 60 kWh/m^3 exhibited a pronounced peak near 2.6 nm. When the microwave energy density exceeded 80 kWh/m^3, the heartwood sample had significantly more mesopores within 10 nm. These results, along with those presented in Figs. 4 and 5, underscored that the damages induced by HIMW treatment in the micro-mesoporous pore structure of the radiata pine sapwood and heartwood were concentrated at the pit borders and torus-margo membrane of the bordered pits, and the damage type was slit-shaped pores with a pore size of less than 10 nm.

Figure 8 shows the proportion of different pore size ranges of the samples before and after the HIMW treatment measured by low-temperature ^{1}H NMR. Notably, the micro-mesopore size distribution of the treated sapwood did not change significantly when the microwave energy densities were 60 kWh/m^3 and 80 kWh/m^3. However, treatment at an energy density of 100 kWh/m^3 significantly altered the pore size distribution of the micropores and mesopores, distinctly contrasting with the untreated samples. Specifically, the proportion of pore diameters smaller than
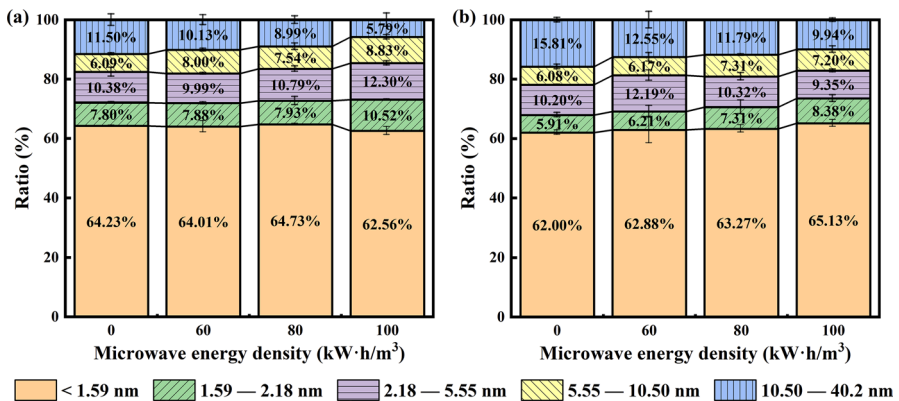

Fig. 8 Micro-mesopore size distributions of untreated and HIMW-treated samples measured by ^{1}H NMR. Sapwood (**a**); Heartwood (**b**)

1.59 nm decreased from 64.23% before the treatment to 62.56% after the treatment, while the proportion of pore diameters in the range of 1.59–10.50 nm increased significantly. The proportions of pores with diameters of 1.59–2.18 nm, 2.18–5.55 nm, and 5.55–10.50 nm were 34.87%, 18.50%, and 45.5% higher, respectively, after the HIMW treatment. This result indicated that the HIMW treatment damaged the weak phase structure, such as the pit membrane of the bordered pits in the cell walls of radiata pine sapwood (Fig. 4). However, the proportion of micropores in the treated heartwood was positively correlated with the microwave energy density. With the microwave energy density reaching 100 kWh/m^3, the proportion of micropores increased from 67.91% (untreated heartwood sample) to 73.51%, reflecting an increase of 8.25%. This shift which might be related to the increased inter-microfibril spaces, was attributed to the HIMW treatment. Furthermore, as depicted in Fig. 8b, the HIMW treatment had a more significant effect on the mesopore size distribution in the heartwood than in the sapwood samples, consistent with the results of the nitrogen adsorption test. The proportion of mesopores with a diameter of less than 10.50 nm in the heartwood after the treatment at 60 kWh/m^3 energy density was 18.36%, which was 12.78% higher than that of the untreated sample. The proportion of pores with a diameter ranging from 2.18 to 5.55 nm witnessed a considerable increase of 19.51%, indicating the most substantial expansion within the smaller mesopores range. However, as the microwave energy density increased further, the proportion of mesopores below a diameter of 10.50 nm showed a decline to 16.55% (the 100 kWh/m^3 treated sample), nearly approaching the proportion found in the untreated samples. The possible reason was the rapid evaporation of moisture from the wood under the electromagnetic field of higher microwave energy density, which generated higher temperatures and vapor pressure in the low-permeability heartwood (Ouertani et al. 2015). Consequently, the degradation of the chemical compositions within cell walls occurred, accompanied by a reduction in mechanical strength, which in turn caused extensive macroscopic damages to the heartwood cell walls (Guo et al. 2015; Zhang et al. 2016).

Certain mesoscopic pores tend to close during wood drying due to capillary tension (Fengel 1970), changing the pore size distribution on the wood cell walls (Grigsby et al. 2013; Li and Zhao 2020). As a result, there are slight differences between the NAD and ^{1}H NMR results. Nonetheless, the NAD and ^{1}H NMR results were consistent and adequately elucidated the impact of the HIMW treatment on the micro-mesopore size distribution of radiata pine sapwood and heartwood.

Macropore structure

The MIP results of the total intrusion volume, pore diameter, and porosity of the radiata pine sapwood and heartwood before and after the HIMW treatment are summarized in Table 6. The values of the pore characteristics of radiata pine heartwood were smaller than those of the sapwood, which was attributed to the structural differences in their physiological functions (Bergstrom 2003). The pore characteristics of the untreated and treated sapwood and heartwood differed substantially. HIMW treatment significantly increased the total intrusion volume and porosity of the

Table 6 Macropore characteristics of untreated and HIMW-treated samples measured by MIP

Sample	Total intrusion volume (mL/g)	Total pore area (m²/g)	Median pore diameter (volume) (nm)	Average pore diameter(4V/A) (nm)	Porosity (%)
S0	1.376	1.877	9451.36	2932.68	61.40
S60	1.384	0.701	8674.09	7897.22	62.39
S80	1.636	0.851	8849.84	7689.58	66.31
S100	1.659	0.737	10,593.09	9011.26	68.56
H0	1.245	1.039	1340.55	374.70	57.11
H60	1.606	2.837	2629.48	343.33	62.69
H80	1.557	7.645	2446.79	814.68	68.10
H100	1.634	13.397	2313.36	487.78	68.98

*The values are given as averages over two samples in one test

wood. The total intrusion volume of the sapwood increased from 1.376 (untreated) to 1.659 mL/g (treated at the energy density of 100 kWh/m³), representing a 20.57% increase, and the porosity increased from 61.40 to 68.56%, an increase of 11.66%. Interestingly, the HIMW treatment exhibited a more pronounced effect on the pore characteristics of the heartwood than on the sapwood. As the microwave energy density increased to 100 kWh/m³, the total intrusion volume of the heartwood increased from 1.245 to 1.634 mL/g, an increase of 31.24%, and the porosity increased from 57.11 to 68.98%, an increase of 20.78%. The significant increases in porosity observed in both sapwood and heartwood can be attributed to the rapid heating of water in wood under the influence of the microwave energy field. This heat leads to the evaporation of water into abundant vapor. The permeability of heartwood was relatively low, thus causing a buildup of high vapor pressure inside the heartwood cells. When the vapor pressure was higher than the strength of the weakest wood structure, various degrees of damage occurred, resulting in a significant increase in wood porosity (Fan et al. 2022; Weng et al. 2020). In addition, the permeability of the wood is primarily influenced by the macropore structure (Tan et al. 2020), which, in turn, accounts for the marked rise in the number of macropores in the HIMW-treated wood. This underlying reason aligns with the observed higher gas permeability in the treated wood, as previously discussed in Sect. "Results of gas permeability test".

Table 6 lists the median pore diameter and average pore diameter of both radiata pine sapwood and heartwood before and after the HIMW treatment. The results demonstrate that different microwave energy densities had complex effects on the wood pore structure. The diameter of median pores in the treated sapwood samples exhibited a reduction when compared to the untreated wood, for both energy densities of 60 kWh/m³ and 80 kWh/m³. However, the average pore diameters demonstrated a substantial increase of 169.28% and 162.20% for the respective energy densities. In addition, the HIMW treatment led to an increase in both median pore diameter and the average pore diameter of the treated heartwood. Figure 9 illustrates these changes in the pore structure of wood in detail caused by HIMW treatment.

Figure 9a shows that the pore size of the untreated sapwood ranged from 1000 to 38,000 nm, with two peaks at 6100 nm and 24,800 nm, corresponding to the bordered pits and tracheids in the wood microstructure (Kvist et al. 2020). The peak at 6100 nm shifted to the right to 7400 nm after the HIMW treatment. As the microwave energy density increased, the peak width increased in the 5000–12,500 nm range, indicating that the HIMW treatment had damaged the bordered pits and CML in the early wood tracheids (Fig. 4 f, i). In addition, it should be noted that the energy density of 100 kWh/m^3 caused macroscopic damage to the internal structure of the sapwood, and the pore size distribution ranged from 120,000 to 220,000 nm. This result could be attributed to the destruction of the intercellular layer situated between the axial tracheids and the ray parenchyma cells, as observed from the effects of the HIMW treatment depicted in Fig. 4i, j.

As shown in Fig. 9b, the pore size of the untreated radiata pine heartwood was in the range of 100–20,000 nm, with three peaks at 180 nm, 1500 nm, and 6000 nm, corresponding to pores in the pit membranes of the bordered pits, pit apertures, and tracheid structures, respectively (Kvist et al. 2020). The pore size underwent complex changes during the HIMW treatment, and the pore size distribution curve exhibited irregular changes. Specifically, the pore size curve of the wood treated with an energy density of 60 kWh/m^3 was M-shaped, and the peak near 180–200 nm was significantly higher, indicating that the HIMW treatment damaged the borders of bordered pits in the longitudinal tracheids. Following the treatment, a reduction was observed in the number of pores within the 680 nm to 6000 nm diameter range, while there was a significant increase in the number of pores with a diameter exceeding 6200 nm. This alteration was attributed to the separation of CML and the destruction of ray parenchyma cells, as visible in Fig. 5e, f. In the case of the sample treated with an energy density of 80 kWh/m^3, the pore size curve exhibited an A-shaped profile, with pore sizes concentrating within the 1400–5000 nm range. The results indicated that the pit apertures of the bordered pits, cell wall layers (CML, S1/S2 layer) of the heartwood longitudinal tracheids, and ray parenchyma cells were adversely affected by the HIMW treatment at an energy density of 80 kWh/m^3, as
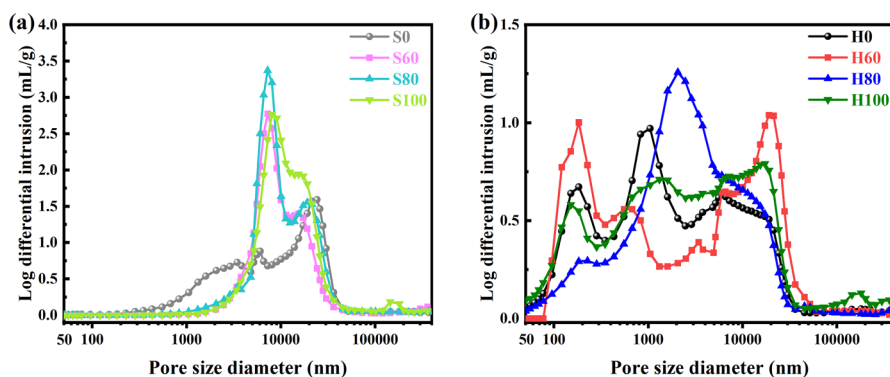

Fig. 9 Log-differential pore size distributions of untreated and HIMW-treated samples measured by MIP. Sapwood (**a**); Heartwood (**b**)

illustrated in Fig. 5g. In addition, the microstructure of the radiata pine heartwood was substantially damaged by the treatment with an energy density of 100 kWh/m^3 (shown in Fig. 5). The porosity of the treated sample was significantly higher than that of the untreated sample, and most of the damaged pores were concentrated within the macropore ranges of 6000–25,000 nm and 85,000–240,000 nm. These changes in pore size distribution corresponded to the separation of the tracheid wall layers, the disruption of cross-field pits, and the radial cracks that were visibly evident due to the damages inflicted upon the ray parenchyma cells, as depicted in Fig. 5h, i. These findings underscored the relationship between the extent of cell structure damage within the heartwood and the increasing microwave energy density, which is associated with the generation of heat through the moisture present in the wood.

Conclusion

This study investigated the effects of HIMW treatment at various energy densities (0, 60, 80, and 100 kWh/m^3) on the gas permeability and the pore size distribution of radiata pine sapwood and hardwood. Through a comprehensive approach involving SEM, NAD, ^{1}H NMR, and MIP techniques, the alterations in the multi-scale pore size distribution after the HIMW treatment were analyzed. The water in the wood cell walls and cell lumen was rapidly vaporized during the treatment. As the vapor pressure increased, the weaker structures were damaged, uniformly improving the wood permeability quickly and efficiently. As the microwave energy density increased, the gas permeability of the wood in the longitudinal, radial, and tangential directions increased significantly. That of the sapwood increased about twofold, and that of the heartwood increased more than sixfold. The combined outcomes of the NAD and ^{1}H NMR analyses within the micro-mesopore diameter range illustrated a noteworthy increase in the BJH average pore diameter for both sapwood and heartwood samples, alongside a reduction in the total pore volume. However, the BET surface area of the sapwood sample increased slightly, whereas that of the heartwood samples decreased. The pore size was significantly larger after the HIMW treatment, and the dominant pores were slit-shaped mesopores with a diameter of less than 10 nm. The MIP results for the macropore range showed that the HIMW treatment had a more pronounced effect on the heartwood than the sapwood. The total intrusion volume and porosity of the treated heartwood were higher than that of the treated sapwood. The macropore diameters in the treated sapwood were in the range of 5000–12,500 nm, and those of the treated heartwood were 6000–25,000 nm and 85,000–240,000 nm. These results were validated by SEM observations. The HIMW treatment led to the destruction of weaker structures, such as pits, cell well layers, and ray parenchyma cells. In summary, the HIMW treatment had a significant effect on the multi-scale pore size distribution of radiata pine sapwood and heartwood, with a more pronounced impact observed in the heartwood. The treatment significantly enhanced the gas permeability of wood due to its effect on the porosity. The results improve our understanding of the effect and mechanism of the HIMW

treatment on the wood structure and provide a theoretical foundation for advancing the HIMW treatment's potential for high-value utilization of wood materials.

Author contributions XX was involved in conceptualization, writing—original draft, investigation, methodology, visualization, and writing—review and editing. SL contributed to conceptualization, methodology, validation, writing—review and editing, and funding acquisition. JJ was involved in validation, writing—review and editing, linguistic assistance. LL and YZ contributed to conceptualization, Writing—review and editing. LP was involved in conceptualization and project administration. FF contributed to resources and supervision.

Declarations

Conflict of interest The authors declare that they have no conflict of interest.

References

Abe I, Fukuhara T, Iwasaki S et al (2001) Development of a high density carbonaceous adsorbent from compressed wood. Carbon 39(10):1485–1490. https://doi.org/10.1016/S0008-6223(00)00273-6

Anovitz LM, Cole DR (2015) Characterization and analysis of porosity and pore structures. Rev Mineral Geochem 80(1):61–164. https://doi.org/10.2138/rmg.2015.80.04

Bamber RK (1976) Heartwood, its function and formation. Wood Sci Technol 10(1):1–8

Bao M, Huang X, Jiang M, Yu W, Yu Y (2017) Effect of thermo-hydro-mechanical densification on microstructure and properties of poplar wood (*Populus tomentosa*). J Wood Sci 63(6):591–605. https://doi.org/10.1007/s10086-017-1661-0

Bergstrom B (2003) Chemical and structural changes during heartwood formation in *Pinus sylvestris*. Forestry 76(1):45–53. https://doi.org/10.1093/forestry/76.1.45

Boonstra MJ, van Acker J, Kegel E, Stevens M (2007) Optimisation of a two-stage heat treatment process: durability aspects. Wood Sci Technol 41(1):31–57. https://doi.org/10.1007/s00226-006-0087-4

Cao H, Lyu J, Zhou Y, Gao X (2021) The study of bound water status and pore size distribution of Chinese fir and poplar cell wall by low-field NMR. Int J Polym Sci 2021:1–11. https://doi.org/10.1155/2021/4954837

Chai Y, Liang S, Zhou Y, Lin L, Fu F (2020) Low-melting-point alloy integration into puffed wood for improving mechanical and thermal properties of wood–metal functional composites. Wood Sci Technol 54(3):637–649. https://doi.org/10.1007/s00226-020-01174-5

Fan Z, Peng L, Liu M, Feng Y, He J, Wu S (2022) Analysis of influencing factors on sound absorption capacity in microwave-treated *Pinus radiata* Wood. Eur J Wood Prod 80(4):985–995. https://doi.org/10.1007/s00107-021-01774-3

Farajollah PM, Edalat H, Valizadeh Kiamahalleh M, Doost Hoseini K (2021) Microwave-assisted laminated veneer lumber (LVL): investigation on the effect of preheating time and moisture content on resin penetration and bonding quality. Constr Build Mater 304:124677. https://doi.org/10.1016/j.conbuildmat.2021.124677

Fengel D (1970) The ultrastrueture of cellulose from wood part 2: problems of the isolation of cellulose. Wood Sci Technol 4:15–35. https://doi.org/10.1007/BF00356234

Furó I, Daicic J (1999) NMR cryoporometry: a novel method for the investigation of the pore structure of paper and paper coatings. Nord Pulp Pap Res J 14(3):221–225. https://doi.org/10.3183/npprj-1999-14-03-p221-225

Ganguly S, Balzano A, Petrič M et al (2021) Effects of different energy intensities of microwave treatment on heartwood and sapwood microstructures in Norway spruce. Forests 12(5):598. https://doi.org/10.3390/f12050598

Gao X, Zhuang S, Jin J, Cao P (2015) Bound water content and pore size distribution in swollen cell walls determined by NMR technology. BioResources 10(4):8208–8224. https://doi.org/10.15376/biores.10.4.8208-8224

Giacomozzi D, Joutsimo O, Zelinka SL (2019) The processing of *Pinus radiata*: pore size distribution changes in the cell wall structure studied by pressure plate technique and mercury intrusion porosimetry. BioResources 14(2):2827–2841. https://doi.org/10.15376/biores.14.2.2827-2841

Grigsby WJ, Kroese H, Dunningham EA (2013) Characterisation of pore size distributions in variously dried *Pinus radiata*: analysis by thermoporosimetry. Wood Sci Technol 47(4):737–747. https://doi.org/10.1007/s00226-013-0537-8

Guo J, Song K, Salmen L, Yin Y (2015) Changes of wood cell walls in response to hygro-mechanical steam treatment. Carbohyd Polym 115:207–214. https://doi.org/10.1016/j.carbpol.2014.08.040

Hao X, Yu C, Zhang G, Li X, Wu Y, Lv J (2020) Modeling moisture and heat transfer during superheated steam wood drying considering potential evaporation interface migration. Dry Technol 38(15):2055–2066. https://doi.org/10.1080/07373937.2019.1662801

He S, Lin L, Fu F, Zhou Y, Fan M (2014) Microwave treatment for enhancing the liquid permeability of Chinese fir. BioResources 9(2):1924–1938. https://doi.org/10.15376/biores.9.2.1924-1938

Jang E, Kang C (2019) Changes in gas permeability and pore structure of wood under heat treating temperature conditions. J Wood Sci. https://doi.org/10.1186/s10086-019-1815-3

Jang E, Yuk J, Kang C (2020) An experimental study on change of gas permeability depending on pore structures in three species (hinoki, Douglas fir, and hemlock) of softwood. J Wood Sci 66(1):789. https://doi.org/10.1186/s10086-020-01925-9

Junghans K, Niemz P, Bächle F (2005) Untersuchungen zum Einfluss der thermischen Vergütung auf die Porosität von Fichtenholz. (Investigations into the influence of thermal treatment on the porosity of spruce). Holz Roh-Werkst 63(3):243–244. https://doi.org/10.1007/s00107-004-0553-3

Kaack L, Altaner CM, Carmesin C et al (2019) Function and three-dimensional structure of intervessel pit membranes in angiosperms: a review. IAWA J 40(4):673–702. https://doi.org/10.1163/22941932-40190259

Kekkonen PM, Ylisassi A, Telkki V (2014) Absorption of water in thermally modified pine wood as studied by nuclear magnetic resonance. J Phys Chem C 118(4):2146–2153. https://doi.org/10.1021/jp411199r

Kojiro K, Miki T, Sugimoto H, Nakajima M, Kanayama K (2010) Micropores and mesopores in the cell wall of dry wood. J Wood Sci 56(2):107–111. https://doi.org/10.1007/s10086-009-1063-z

Kol HŞ, Çayır B (2023) The effects of increasing preservative uptake by microwave pre-treatment on the microstructure and mechanical properties of Oriental spruce wood. Wood Mat Sci Eng 18(2):732–738. https://doi.org/10.1080/17480272.2022.2077656

Kvist P, Gebäck T, Rasmuson A (2020) A multi-scale model for diffusion of large molecules in steam-exploded wood. Wood Sci Technol 54(4):821–835. https://doi.org/10.1007/s00226-020-01185-2

Lehringer C, Richter K, Schwarze F W, Militz H (2009) A review on promising approaches for liquid permeability improvement in softwoods. Wood Fiber Sci 373–385

Li X, Zhao Z (2020) Time domain-NMR studies of average pore size of wood cell walls during drying and moisture adsorption. Wood Sci Technol 54(5):1241–1251. https://doi.org/10.1007/s00226-020-01209-x

Li W, Chen Z, Yu H, Li J, Liu S (2021) Wood-derived carbon materials and light-emitting materials. Adv Mater 33(28):e2000596. https://doi.org/10.1002/adma.202000596

Liang R, Zhu Y, Wen L et al (2020) Exploration of effect of delignification on the mesopore structure in poplar cell wall by nitrogen absorption method. Cellulose 27(4):1921–1932. https://doi.org/10.1007/s10570-019-02921-z

Maloney TC, Paulapuro H, Stenius P (1998) Hydration and swelling of pulp fibers measured with differential scanning calorimetry. Nord Pulp Pap Res J 13(1):31–36. https://doi.org/10.3183/npprj-1998-13-01-p031-036

Muller ACA, Scrivener KL (2017) A reassessment of mercury intrusion porosimetry by comparison with ^{1}H NMR relaxometry. Cem Concr Res 100:350–360. https://doi.org/10.1016/j.cemconres.2017.05.024

Östlund Å, Köhnke T, Nordstierna L, Nydén M (2010) NMR cryoporometry to study the fiber wall structure and the effect of drying. Cellulose 17(2):321–328. https://doi.org/10.1007/s10570-009-9383-0

Ouertani S, Hassini L, Azzouz S, Torres SS, Belghith A, Koubaa A (2015) Modeling of combined microwave and convective drying of wood: prediction of mechanical behavior via internal gas pressure. Dry Technol 33(10):1234–1242. https://doi.org/10.1080/07373937.2015.1022828

Park S, Venditti R, Jameel H, Pawlak J (2006) Changes in pore size distribution during the drying of cellulose fibers as measured by differential scanning calorimetry. Carbohyd Polym 66(1):97–103. https://doi.org/10.1016/j.carbpol.2006.02.026

Poonia PK, Hom SK, Sihag K, Tripathi S (2016) Effect of microwave treatment on longitudinal air permeability and preservative uptake characteristics of chir pine wood. Maderas Ciencia y Tecnología 18(1):125–132. https://doi.org/10.4067/S0718-221X2016005000013

Ramezanpour M, Tarmian A, Taghiyari HR (2015) Improving impregnation properties of fir wood to acid copper chromate (ACC) with microwave pre-treatment. iForest Biogeoscis for 8(1):89–94. https://doi.org/10.3832/ifor1119-007

Sang G, Liu S, Zhang R, Elsworth D, He L (2018) Nanopore characterization of mine roof shales by sans, nitrogen adsorption, and mercury intrusion: impact on water adsorption/retention behavior. Int J Coal Geol 200:173–185. https://doi.org/10.1016/j.coal.2018.11.009

Song Z, Jing C, Yao L et al (2016) Microwave drying performance of single-particle coal slime and energy consumption analyses. Fuel Process Technol 143:69–78. https://doi.org/10.1016/j.fuproc.2015.11.012

Tan Y, Hu J, Chang S et al (2020) Relationship between pore structure and gas permeability in poplar (*Populus deltoides* CL '55/65') tension wood. Ann Forest Sci 77(3):234. https://doi.org/10.1007/s13595-020-00994-6

Tanaka T, Avramidis S, Shida S (2010) A preliminary study on ultrasonic treatment effect on transverse wood permeability. Maderas Ciencia y Tecnología 12(1):3–9. https://doi.org/10.4067/S0718-221X2010000100001

Tanikawa W, Shimamoto T (2009) Comparison of Klinkenberg-corrected gas permeability and water permeability in sedimentary rocks. Int J Rock Mech Min 46(2):229–238. https://doi.org/10.1016/j.ijrmms.2008.03.004

Telkki V, Yliniemi M, Jokisaari J (2013) Moisture in Softwoods: fiber saturation point, hydroxyl site content, and the amount of micropores as determined from NMR relaxation time distributions. Holzforschung 67(3):291–300. https://doi.org/10.1515/hf-2012-0057

Terziev N, Daniel G, Torgovnikov G, Vinden P (2020) Effect of microwave treatment on the wood structure of Norway spruce and radiata pine. BioResources 15(3):5616–5626. https://doi.org/10.15376/biores.15.3.5616-5626

Torgovnikov G, Vinden P (2009) High-intensity microwave wood modification for increasing permeability. Forest Prod J 59(4):84–92

Torgovnikov G, Vinden P (2010) Microwave wood modification technology and its applications. Forest Prod J 60(2):173–182. https://doi.org/10.13073/0015-7473-60.2.173

Vinden P, Torgovnikov G, Hann J (2011) Microwave modification of Radiata pine railway sleepers for preservative treatment. Eur J Wood Prod 69(2):271–279. https://doi.org/10.1007/s00107-010-0428-8

Wang G, Wang K, Ren T (2014) Improved analytic methods for coal surface area and pore size distribution determination using 77K nitrogen adsorption experiment. Int J Min Sci Technol 24(3):329–334. https://doi.org/10.1016/j.ijmst.2014.03.007

Wang Z, Xu E, Fu F, Lin L, Yi S (2022) Characterization of wood cell walls treated by high-intensity microwaves: effects on physicochemical structures and micromechanical properties. Ind Crop Prod 187:115341. https://doi.org/10.1016/j.indcrop.2022.115341

Weng X, Zhou Y, Fu Z, Gao X, Zhou F, Fu F (2020) Effects of microwave treatment on microstructure of Chinese fir. Forests 11(7):772. https://doi.org/10.3390/f11070772

Xu E, Lin L, Li S, Peng L, Zhou Y, Fu F (2020) Wood microwave treatment technology and its applications. China Wood Industry 34(1):20–24+29. https://doi.org/10.19455/j.mcgy.20200105

Yang X, Pang X, Liu X, Yang S, Li X (2023) Determining the pore structure and radial variability of moso bamboo (*Phyllostachys edulis*). Wood Sci Technol 57(2):345–357. https://doi.org/10.1007/s00226-022-01451-5

Yin J, Song K, Lu Y, Zhao G, Yin Y (2015) Comparison of changes in micropores and mesopores in the wood cell walls of sapwood and heartwood. Wood Sci Technol 49(5):987–1001. https://doi.org/10.1007/s00226-015-0741-9

Yongsawatdigul J, Gunasekaran S (1996) Microwave-vacuum drying of cranberries: part i. Energy use and efficiency. J Food Process Pres 20(2):121–143. https://doi.org/10.1111/j.1745-4549.1996.tb00850.x

Zauer M, Kretzschmar J, Großmann L, Pfriem A, Wagenführ A (2014) Analysis of the pore-size distribution and fiber saturation point of native and thermally modified wood using differential scanning calorimetry. Wood Sci Technol 48(1):177–193. https://doi.org/10.1007/s00226-013-0597-9

Zhang X, Han G, Jiang W, Zhang Y, Li X, Li M (2016) Effect of steam pressure on chemical and structural properties of kenaf fibers during steam explosion process. BioResources 11(3):6590–6599. https://doi.org/10.15376/biores.11.3.6590-6599